Productivity Optimization of Oil Wells Using a New 3D Finite-Element Wellbore Inflow Model and Artificial Neural Network

M. A. Proett, J. Ansah, M. Y. Soliman, R. Schultz, and K. Folse

Halliburton Energy Services, Inc.

Abstract

The most common method of completing a well involves cementing a steel casing in the well bore and then using shaped charges to perforate the casing and penetrate the producing zone. The productivity of these wells is influenced by several factors, which include the length of the individual perforations, casing entrance hole diameter, perforation shot density, phase angle between the perforations, and the degree of damage inside and around the perforations.

This paper presents application of a new wellbore inflow model to quantify the effects of these individual parameters on productivity. This model incorporates the cone-shaped perforation geometry with a tapered tip that has been observed in the laboratory for years. For the first time, the asymmetric, spiral distribution of perforations around a wellbore is modeled using a full 3-dimensional finite element model with over 30,000 elements in each perforation layer instead of the 2-dimensional and quasi 3-dimensional models used in the past. In addition, the wellbore inflow model is used to study the effect of reservoir anisotropy and dip angle of the bedding planes on perforation design over a wide range of shot densities and phasing.

Productivity results from the new 3D model are compared with previous models to demonstrate the improvements to the inflow predictions. The effect of reservoir anisotropy on perforation design is also studied over a wide range of shot densities and phasing. Results that highlight the effect of reservoir anisotropy are presented in this work.

The wellbore inflow model results are also used to develop a neural network algorithm that closely matches the finite element simulation results. This neural network provides an efficient method of evaluating the primary factors that can influence a perforation design and make it possible to optimize the flow performance of cased and perforated wells.

Based on the wellbore inflow model results and the neural network algorithm, the PerfPro™ software product was developed which is used to optimize perforation design of cased and perforated wells. Finally, we demonstrate practical application of PerfPro using a field example.

Introduction

Maximizing the productivity of cased and perforated wells is vital to the success of any field development. The perforation strategy adopted for individual cased wells plays an important role on the well's productivity, and has been a subject of investigation by researchers for decades.[1-3] The enormous interest in this area stems from the fact that cased-hole completions have remained the method of choice over openhole wells. This preference results for several reasons. First, cased and perforated completions have the unique advantage of providing an operator with the flexibility of isolating water-bearing zones from hydrocarbon-bearing zones. Second, cased-hole completions can guarantee long-lasting wellbore integrity. Third, cased and perforated wells provide the unique opportunity for selective exploitation of multiple productive zones in a stratified formation, effective sand control, etc.

However, casing a productive interval creates artificial impairment to fluid flow from the reservoir into a wellbore. Successful perforation should therefore establish an effective communication between the wellbore and the productive formation.

The productivity index of a well is defined as the ratio of production rate, q, to the differential pressure across the formation, ΔP. In the case of an ideal openhole well, productivity index under steady-state conditions is defined by Eq. 1 as:

$$J_{ideal} = \frac{q}{\Delta P} = \frac{2\pi kh}{\mu \ln(r_e / r_w)} \quad \text{..... (1)}$$

In an actual cased well, perforations and formation parameters affect the productivity index. This change in the productivity is expressed as a skin effect, which is the increase (or decrease) in pressure introduced by these factors for a given production.

The ratio of the actual well productivity index to the ideal openhole productivity index is referred to as the productivity ratio (*PR*) and can be expressed in terms of the total skin s_t as follows:

$$PR = \frac{J_{actual}}{J_{ideal}} = \frac{\ln(r_e / r_w)}{\ln(r_e / r_w) + s_t} \quad \text{..... (2)}$$

The variables in Eqs. 1 and 2 are characteristics of the reservoir, and are defined in the nomenclature. The efficiency of a cased and perforated completion is reflected in the value of total skin, s_t, which is a function of several components:

$$s_t = F\left(s_D, s_{pf}, s_{pc}, s_\theta, ...\right) \quad \text{..... (3)}$$

Perforation skin factor, s_{pf}, is a reflection of the effectiveness of the perforation process and its design. The perforation skin factor, skin due to partial penetration, as well as the skin due to well deviation are primarily related to the geometric configuration of the perforations and the wellbore-formation geometry (*e.g.*, height of the perforated zone, formation anisotropy and dip angle). These variables are normally estimated either analytically or numerically.[4-6]

The total skin is usually determined by a pressure transient test. If the other components of the total skin can be determined accurately, the drilling-induced damage, s_D, can then be estimated. Separating the skin damage factor in this fashion enables the efficiency of treatment methods to be evaluated with greater confidence.

Estimates of perforation effectiveness were first made using analytical and electrical analog experiments conducted by Muskat.[1] These fundamental studies showed how well productivity increased with shot density and perforation length.

One of the earliest finite-difference simulations of perforated wells was published by Harris.[2] The author also evaluated the effect of perforation diameter, but his model was limited to all shots being in the same horizontal plane. The first finite element simulations were published by Klotz *et al*.[3] in which both drilling and perforation damages were modeled. Hong[7] continued this work by adding staggered perforations and developed a monograph to determine perforation and skin damage factors.

A commercial finite-element simulator was used by Locke[8] to study the effects of shot density and the extent of drilling damage. The author reported that well productivity improved with increased shot density, and drilling-induced damage can have a significant impact on well productivity. Tariq[9] improved upon Locke's simulator with refinements to the meshing. He reported consistently lower productivity values than Locke's results showed, which was attributed to the increased accuracy. Tariq's mesh was not a full three-dimensional model, however, because, as in previous papers, simplifications were made for phasing other than zero.

In a later study, Karakas and Tariq[6] developed a semi-analytical model correlated with numerical results to investigate the effects of various perforation and reservoir parameters on well productivity. Today most of the estimates of perforated well productivity use these findings.

A finite-difference model was developed recently by Dogulu[10] that coupled a finely gridded near-wellbore model with a larger reservoir simulator. The wellbore model included features for unequal or asymmetrical perforation configurations. Using this coarsely gridded reservoir model coupled to the wellbore grids, slanted and horizontal well completions were evaluated.

Recently Ansah *et al*.[11] presented a model of a spiral and asymmetric distribution of perforations around a wellbore using a full 3-dimensional finite-element model. The authors demonstrated the need for a full 3-

dimensional representation of perforations in the near-wellbore zone when simulating the wide range of perforation scenarios encountered in actual field operations. A cone-shaped geometry was also proposed for describing shaped-charge perforations. Sensitivity analysis conducted in this work shows the effects the new shape parameters have on well productivity.

Procedure 3-D Finite Element Well Inflow Model

Advances in finite element analysis techniques make it feasible to model perforation completions in much greater detail than in previous studies.[7-10] Improved meshing algorithms speed the mesh generation and permit the creation of grids that topologically match the geometry. Increased mesh densities are also possible, without sacrificing solution times. In addition to the increased speed and memory capacity of desktop systems, application of new and more efficient solvers has significantly reduced solution times.

To take advantage of these advances in technology ANSYS was chosen as the finite element code. The thermal diffusion model (Solid70 element), which is completely analogous to Darcy flow in a porous medium, was used. The following partial differential equation is solved using a sparse matrix direct solver:

$$\frac{\partial}{\partial x}\left(k_{xx}\frac{\partial P}{\partial x}\right)+\frac{\partial}{\partial y}\left(k_{yy}\frac{\partial P}{\partial y}\right)+\frac{\partial}{\partial z}\left(k_{zz}\frac{\partial P}{\partial z}\right)=\phi\mu c_t\frac{\partial P}{\partial t} \quad \text{..... (4)}$$

Pressure solutions are generated over a complex finite-element domain, which is comprised of the wellbore, perforations, and the reservoir. Thus, inflow performance of the wells is greatly influenced by:

- length of individual perforations inside the formation, L_p
- entrance hole diameter in the casing, D_{EH}
- density of the perforations (i.e., shot density, SPF), n_p
- angle of phasing between the perforations, θ, and
- degree of damage inside and around the perforation.

In addition to these primary factors, several secondary factors indirectly affect the productivity of cased and perforated wells. These include:

- compressive strength of the porous rock
- effective confining stress, σ
- drilling-induced damage
- effective permeability of the formation, k
- permeability anisotropy, k_v/k_{xy}
- dip angle of the bedding planes, k_v/k_{xy}, as well as
- level of underbalance or overbalance, ΔP, between the formation and the wellbore during perforation.

A parametric model was constructed using the ANSYS application programming language to efficiently generate and solve models covering a wide range of perforating geometries and formation properties. This made it possible to obtain pressure solutions from Eq. 4 simulating Darcy's flow and compute directional velocities and well production rates, which are then used to evaluate well performance.

Major features of the WIM include any number of perforations depending on selected formation thickness and shot density, three-dimensional permeability distribution, as well as multiple pay properties. Maximum perforation shot density allowed is 21 shots per foot. Position of the formation boundaries relative to the perforations can be varied in WIM, which permits simulation of partially perforated completions. Drilling-induced damaged zone is also modeled, as well as crushed zone around the perforations.

Figure 1 shows half of the near-wellbore area of WIM with spiral arrangement of the perforations in the case of a 3-foot reservoir. A segment of this, which covers two adjacent perforations, is presented in Figure 2. Observe the finer mesh around the perforations, especially at the tip where most of the reservoir fluid

enters. The reservoir size was established at 100 times the wellbore diameter, based on a sensitivity analysis to ensure less than 1% error in the solution. A sample plot from this analysis is presented in Figure 3. This figure shows improvement in the solution as the size of the reservoir is increased, although the rate of change in the solution diminishes rapidly.

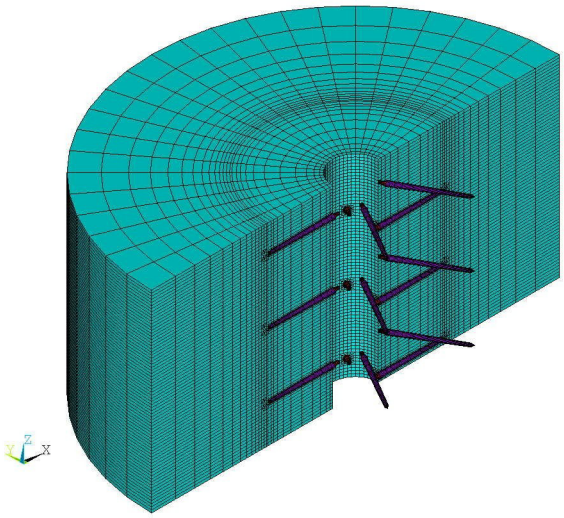

Figure 1. 3D finite element meshes showing a 3-foot section with 6 perforations per foot and 60° phasing

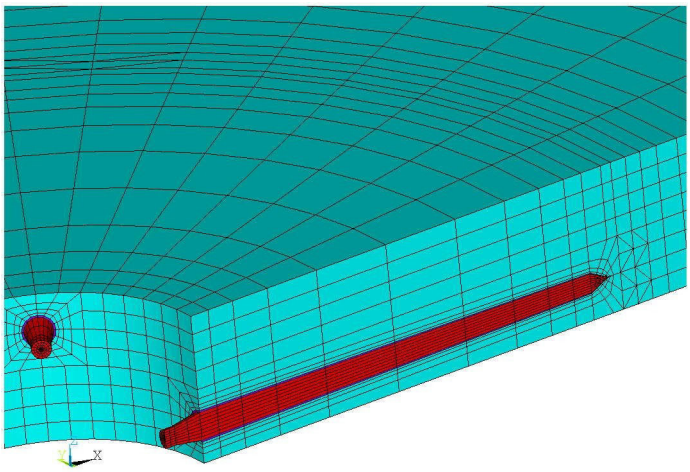

Figure 2. Finite element mesh of the perforation tunnel. The perforation tunnel elements are shown in red, the crushed zone elements are purple, and the formation elements are light blue.

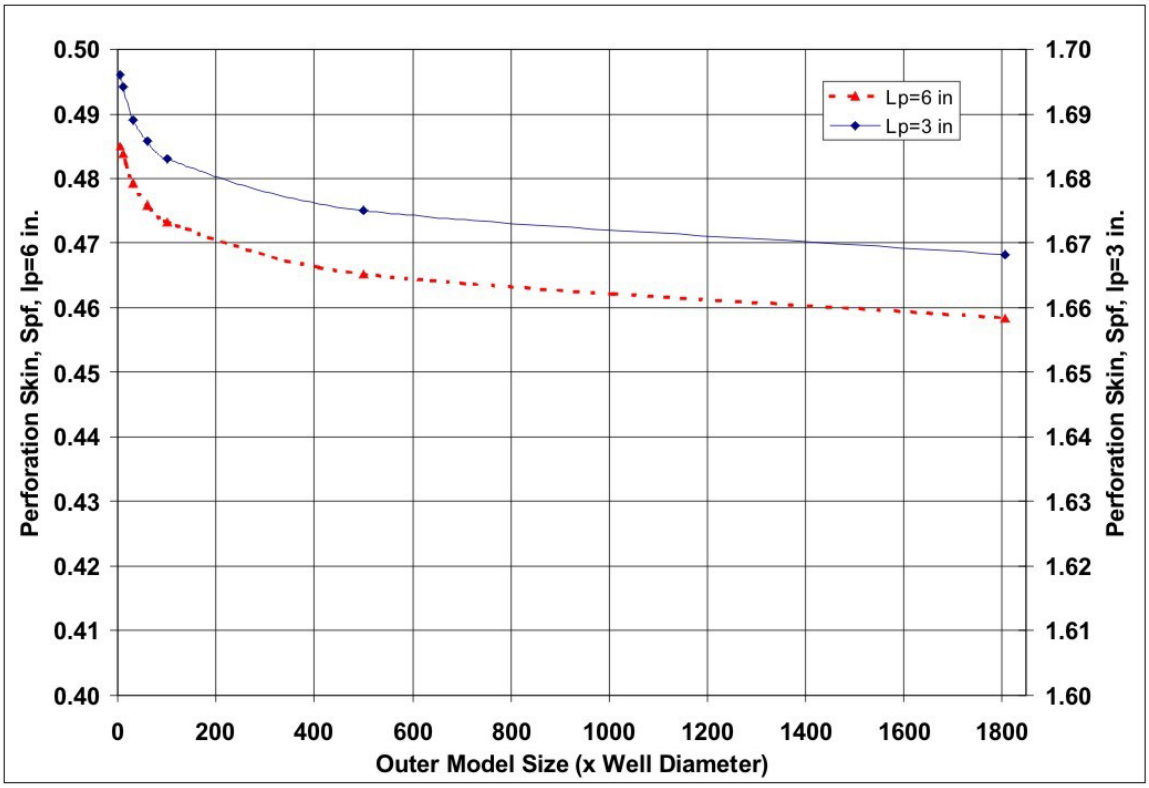

Figure 3. Model size selection: Calculated perforation skin values vs. reservoir size

Similar sensitivity studies were conducted for selecting minimum reservoir thickness. Although WIM is flexible as far as reservoir thickness input, a minimum value of 3 feet was selected for routine analysis. This value, again, ensures approximately 1% or less accuracy goal established for this work. A summary of the results, based on *PR* predictions for 1- to 7-ft thick, fully completed reservoirs, is shown in Figure 4.

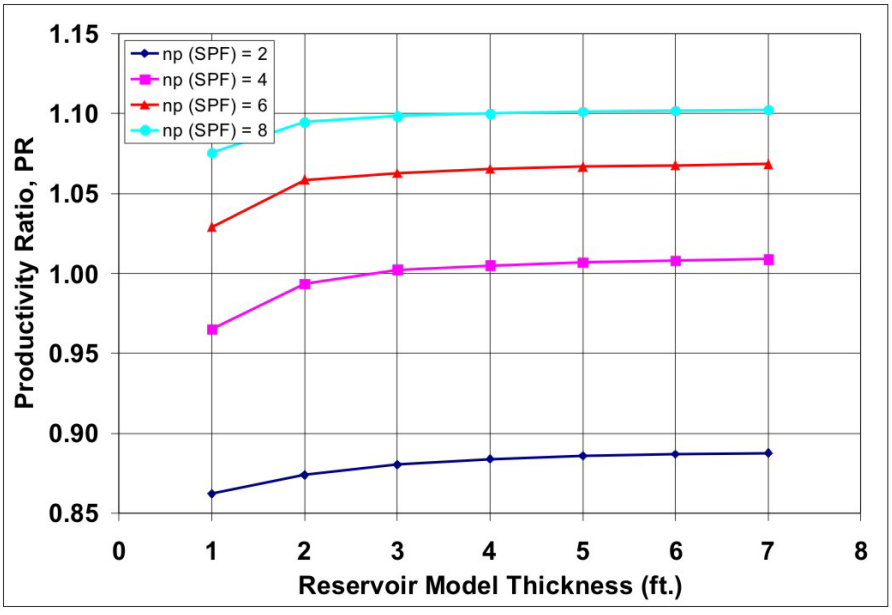

Figure 4. Model thickness selection: Calculated productivity ratio vs. reservoir thickness

One key limiting assumption eliminated in WIM is the use, over the years, of unrealistic cylindrical shaped perforations. Figure 5 shows a typical perforation tunnel inside a 7-inch diameter core. Observe from this two-dimensional view that the shape of the perforation is more of a cone with a convergent tip, rather than a cylinder used in past models. Selection of perforation geometry is documented in Ref. 11 using a perforated core inflow model (PCIM). An extensive study was performed to determine the most representative shape where API RP43 Section IV test[12] results from core samples were matched with the PCIM predictions. Based on the results from the study, a cone-shaped perforation geometry with a tapered tip, Figure 6, was determined to correctly characterize in-situ perforations in terms of the overall shape as well as inflow performance results. It is important to note that D_{EH}, which is usually the most restricted area along the entire perforated tunnel, has a dominant effect on inflow performance of perforations.

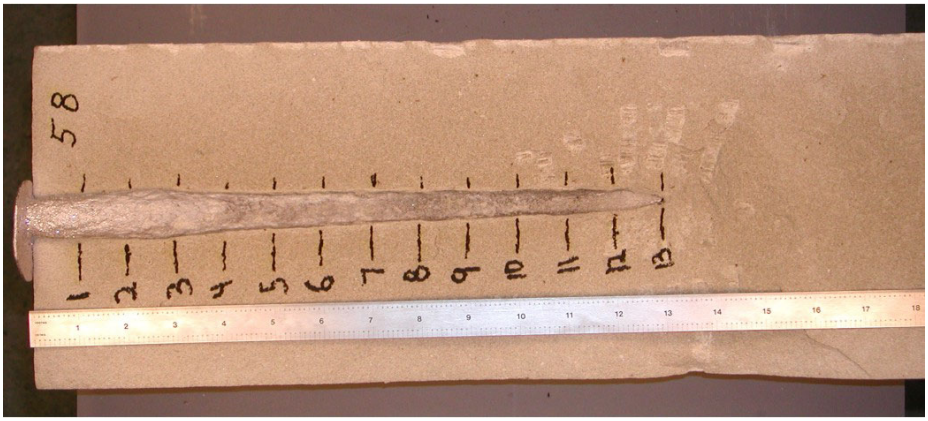

Figure 5. Example core cross-section after API section IV test

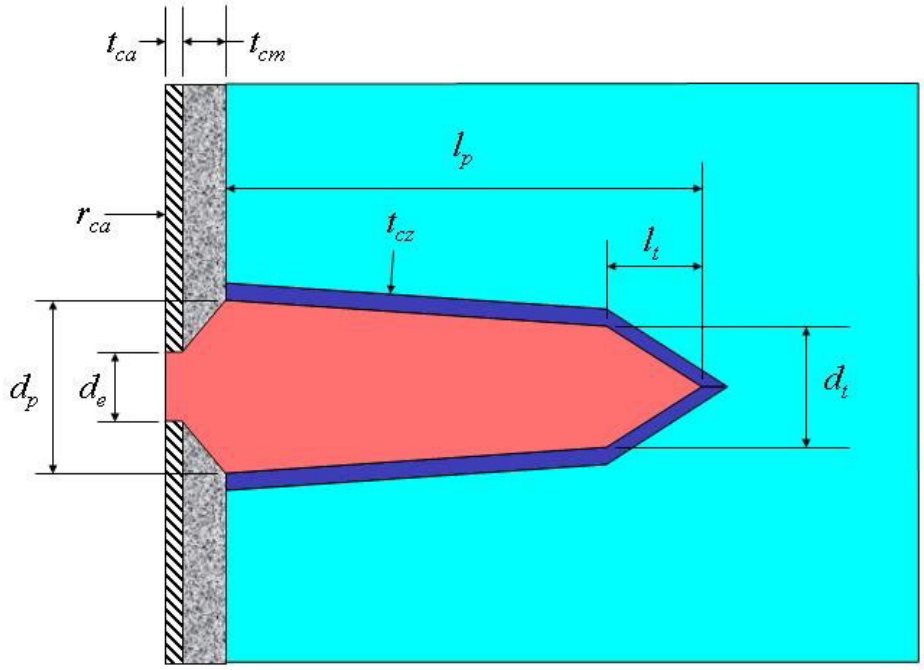

Figure 6. Cone-shaped perforation geometry used in WIM

Another feature about this perforation geometry is the important nature of the tapered perforation tip. This fact was first noted by Howard in Ref. 1, and is especially pertinent in the case of short perforations. This cone-shaped perforation geometry was used in the development of WIM.

Validation of the Well Inflow Model

Detailed validation of WIM is also presented in Ref. 11 using a wide range of casing entrance hole diameters, perforation lengths, and angular phasings, as well as different perforation geometries. The benchmark comparisons were done using cylindrical perforation geometry.

Figure 7 shows WIM predictions of *PR* as a function of perforation length for a well completed with 4 shots per foot at 90° phasing angle. In these simulations, the wellbore radius, r_w, was 0.25 feet and the reservoir drainage radius, r_e, was 660 feet. The cylindrical perforations had D_{EH}=0.5 inches for consistency. The *PR* predictions were compared with laboratory results reported by McDowell and Muskat[1], as well as finite element results generated by Tariq.[9] This figure shows a very good match of Muskat's data for short perforations, as well as Tariq's results for all ranges of perforation lengths. It is important to note that deviation of Muskat's results from *PR* estimates of actual long spirally distributed perforations around a wellbore has been discussed extensively in the past.[1,2]

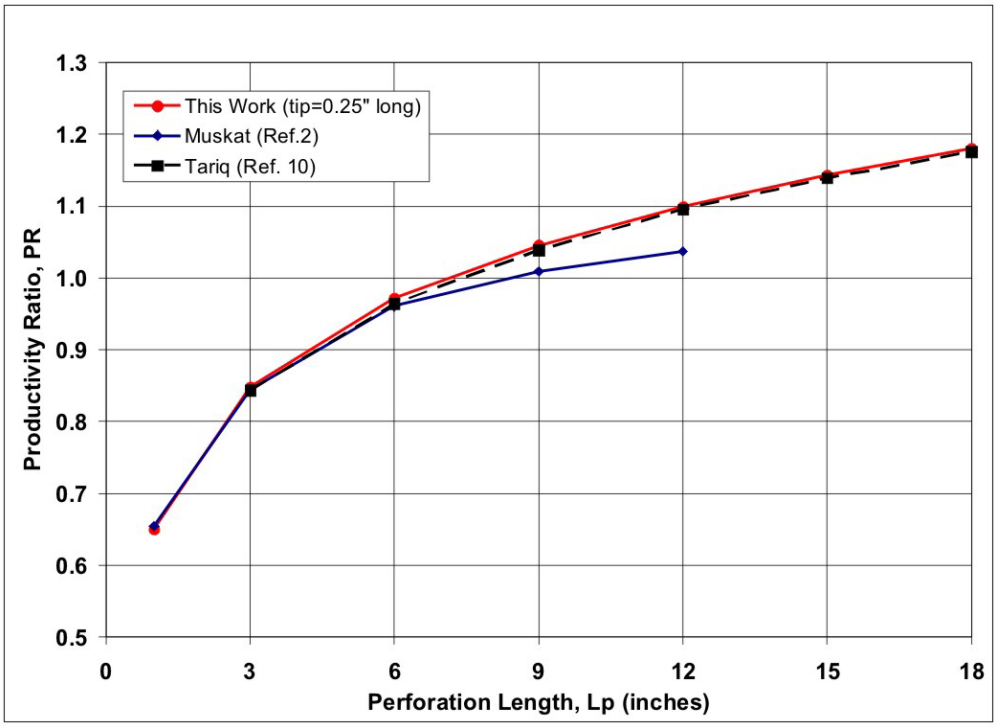

Figure 7. Model validation: Comparison of WIM predictions with productivity ratios from Muskat and Tariq

Pressure distribution within the near-wellbore area is presented in Figure 8. This geometrically complex profile prevents the use of any reasonably small but accurate symmetrical model in lieu of a full 3-dimensional model. Figure 9 shows a comparison of WIM predictions compared with *PR* results from Tariq and Locke's models, which are also based on finite-element analysis. Note that for this comparison, cylindrical perforation geometry was used, as this is the only geometry used in the past models. Certainly, Locke's results are overly optimistic for all the phase angles examined.

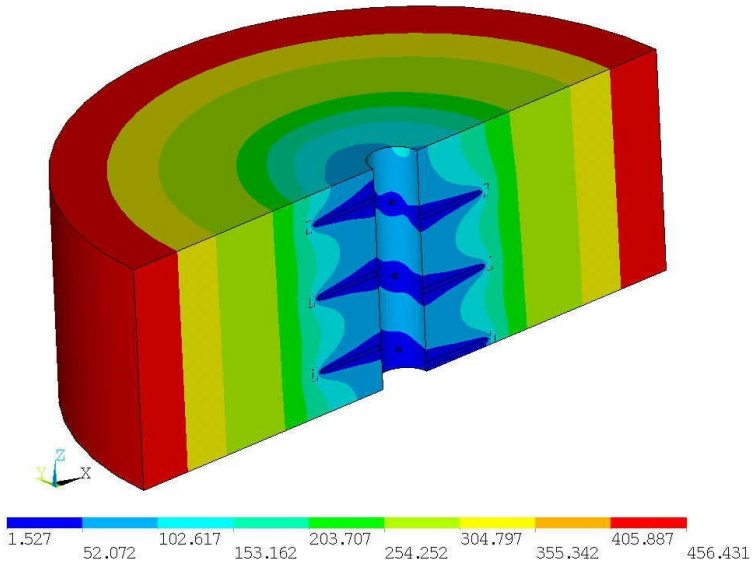

Figure 8. Pressure contour plot for base model

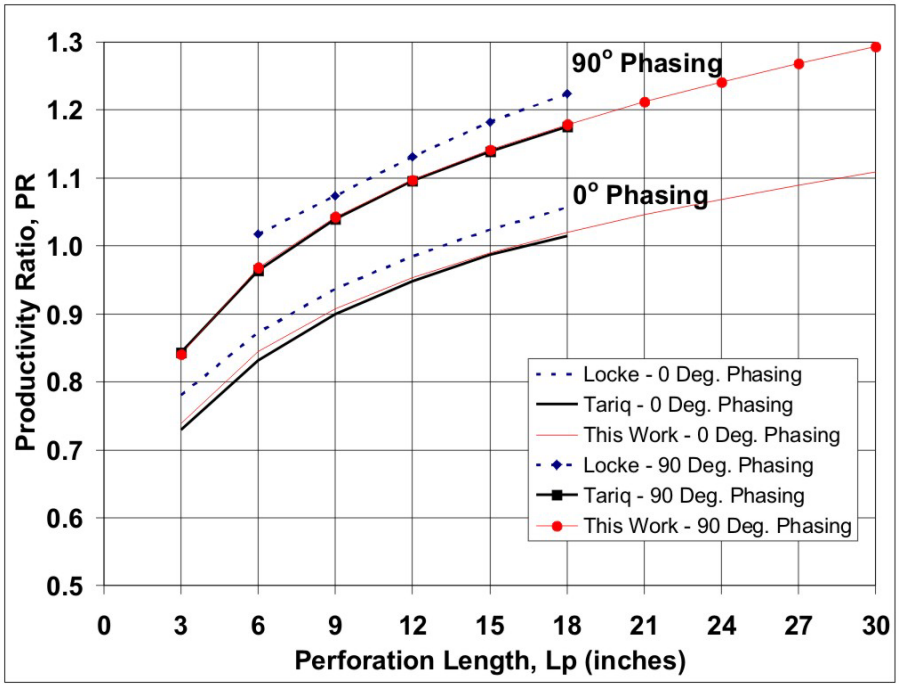

Figure 9. Comparison of WIM predictions with published results for 0° and 90° phasing angles

As was demonstrated in the model thickness selection, however, there is continuous improvement in *PR* predictions with increased model thickness, although the rate of increase reduces significantly. This means, *PR* results will be slightly different depending on the model thickness used. In the past, one-foot model results have been scaled to achieve results for the entire reservoir interval. This technique has been eliminated in WIM, which models all the perforations within a given perforated interval.

Parametric Analysis

In this section, we examine productivity predictions for realistic wellbore perforated completions. Although it is impossible to simulate all potential factors affecting fluid flow in the near-wellbore area in a field, many have been examined with WIM.[11] We examine a few of these findings involving some of the secondary factors listed above.

Figure 10 presents productivity ratio as a function of perforation length for 0^o and also 60^o phasing. In this figure, we show both perforations with and without crushed zones. Two examples are shown in the case of damaged perforations: perforations with crushed zone thickness equal to half the entrance hole diameter and others with crushed zone thickness equal to D_{EH}. The important point from this plot is that it is not adequate to know only the degree of permeability reduction in the crushed zone for optimization of well inflow performance. Good estimate of the thickness of the crushed zone is equally important in this process. Thus, accurate characterization of the crushed zone is essential for optimization of inflow performance of perforated completions.

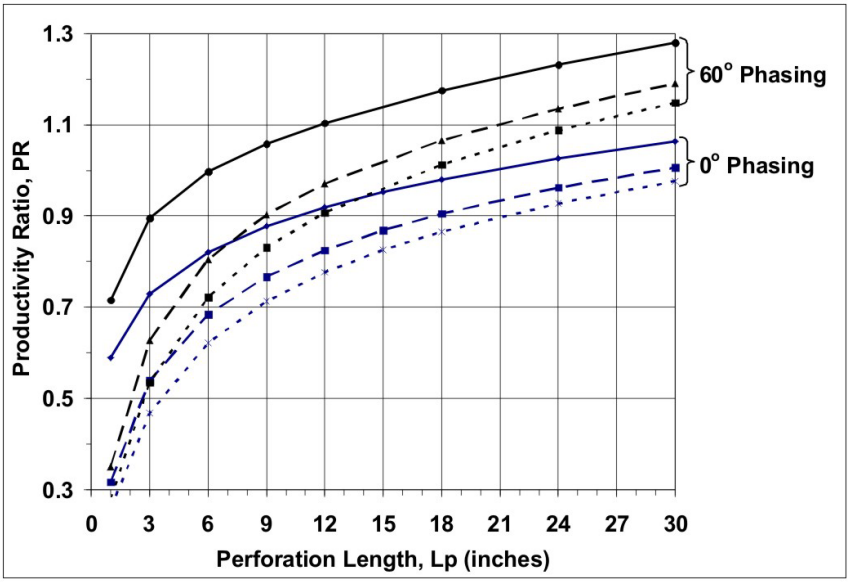

Figure 10. Sensitivity of predicted productivity ratio on crushed zone thickness

The effects of reservoir anisotropy on the base case are illustrated in Figure 11. Anisotropy is defined as k_z/k_{xy} where the vertical permeability k_z is aligned with the wellbore z-axis, and the horizontal permeability k_{xy} is aligned in the horizontal x-y plane. As shown in Figure 11, anisotropy reduces the PR, and thereby, increases the perforation skin. This phenomenon is explained by the fact that each perforation is competing for flow from adjacent perforations. Adjacent perforations are oriented both vertically and horizontally from each other, and the anisotropy in the vertical direction reduces production in this direction. The net result is that anisotropy always reduces the PR and increases skin. Anisotropy normally reflects the sedimentary bedding plane orientation. In vertical wells, it is assumed that the well penetrates the bedding plane perpendicularly so that the anisotropy is oriented with the wellbore. In certain cases, however, the well penetrates the bedding plane at an angle where the dip angle, θ_{dip}, is defined as the deviation from the z-axis. Note that this dip angle is with respect to the reservoir anisotropy, which can occur at any orientation relative to the x or y-axis.

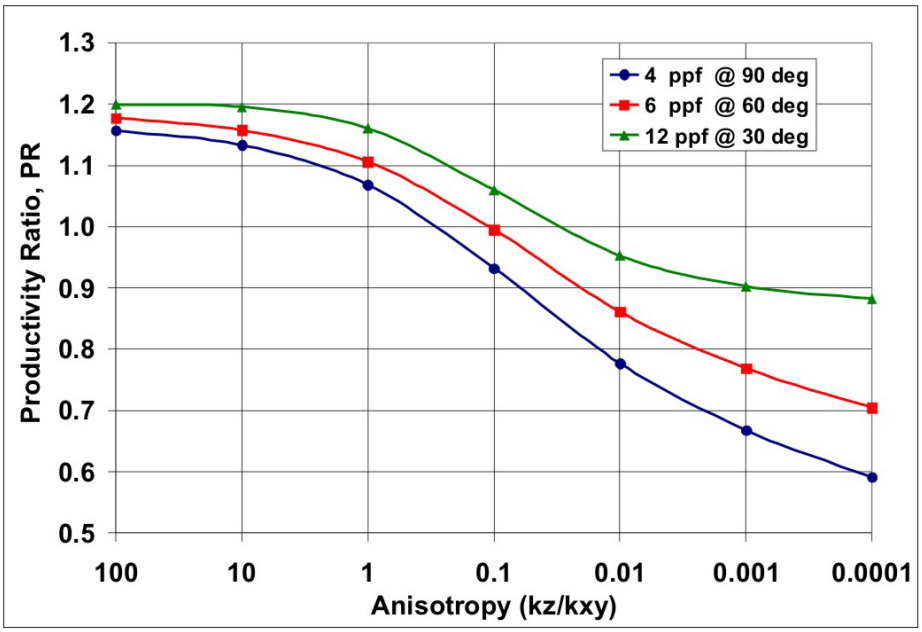

Figure 11. Effect of formation anisotropy and varying perforation densities on well productivity

Figure 12 demonstrates the effect the dip angle has on *PR* for a formation with 0.10 anisotropy and a 45° dip angle. Sensitivity analysis using the base case with k_z/k_{xy}=1.0 is shown by the horizontal line with a *PR* of almost 1.11. It is logical to expect that in an isotropic medium the well productivity is going to remain the same, regardless of re-arrangement of the layers. Pressure distribution for the case with 0.10 anisotropy and 45° dip angle is illustrated in Figure 13.

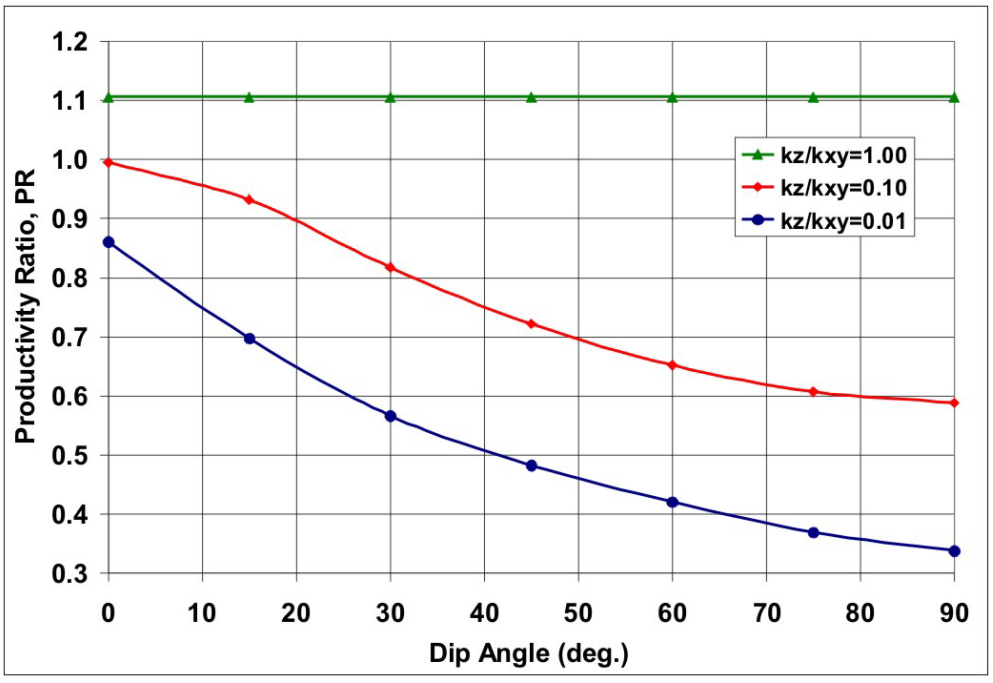

Figure 12. Dip angle sensitivity analysis for varying degrees of anisotropy (base case perforation geometry used)

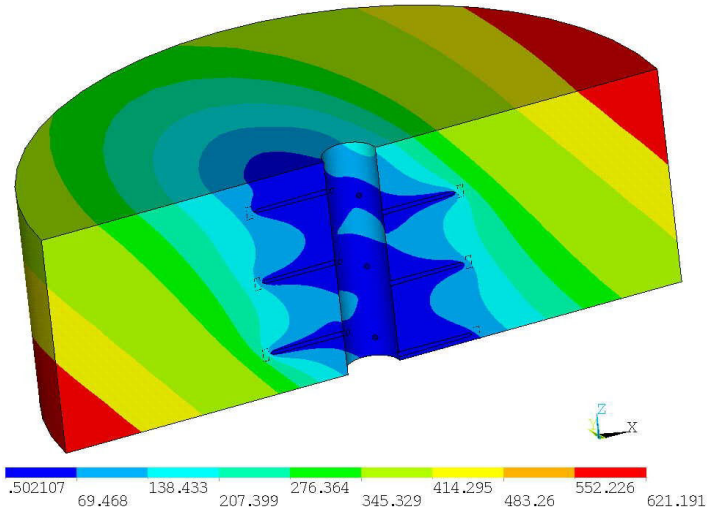

Figure 13. Pressure contour plot with anisotropy of k_x/k_{xy}=0.10 and a dip angle of 45°

As can be recalled from Figure 11, as formation anisotropy decreases, the *PR* is reduced. Figure 12 shows further reduction in the values of *PR* as the dip of the bedding plane is increased from 0° to 90°. For a dip angle of 90°, the permeability aligned with the wellbore is equal to the horizontal permeability k_{xy} of the formation and the vertical permeability k_z is perpendicular to the wellbore. Figure 12 also shows that a dip angle of 90° has the lowest *PR*. In the case of 0.10 anisotropy the *PR* is reduced by as much as 50% and for 0.01 anisotropy by as much as 70% over the isotropic case. Therefore, anisotropy and dip angle are major factors that affect well productivity and total skin.

Productivity Model Using Artificial Neural Network

Results from a parametric study using the new WIM are used to develop a database, which is then used to feed an Artificial Neural Network (ANN) that closely matches the perforation parameters.

A neural network can be generally described as a flexible nonlinear multiple-input, multiple-output mathematical function, which can be adjusted or "tuned" in an organized fashion to emulate a system or process for which an input/output relationship exists. For a given set of input/output data, a neural network is "trained" until a particular input produces a desired output, which matches the response of the system being modeled. After a network is trained, inputs that are not present in the training dataset will produce network outputs that closely match the corresponding outputs of the actual system if the same inputs were applied to the actual system. Neural networks can be devised to produce binary (1/0, yes/no) or continuous outputs.

The key idea is that a mathematical model, which describes a possibly very complex input/output relationship, can be constructed using only data that represents the system being modeled without the development of first principle models. This capability provides a very powerful tool, which can be used to solve a variety of problems in many fields.

In this work, a neural network model was used to capture the relationship between perforation length, entrance hole diameter, length of perforation, number of shots per foot, shot phasing and pseudo-skin associated with the perforated completion. The finite element results from WIM were used as the training data. Neural network training using the Levenberg-Marquardt training algorithm[13] was performed. The network used is a multi-layer feed-forward network consisting of two layers. The first layer contains 20 nonlinear log-sigmoid neurons and the output layer contains a single linear neuron.

Figure 14 shows FEA results along with the neural network results for the base case, in which the wellbore radius, entrance hole diameter and shot density per foot are fixed at 4.25 in., 0.5 in. and 6 SPF, respectively. Eq. 2 was used to calculate corresponding productivity ratio using the ANN predicted perforation skin value.

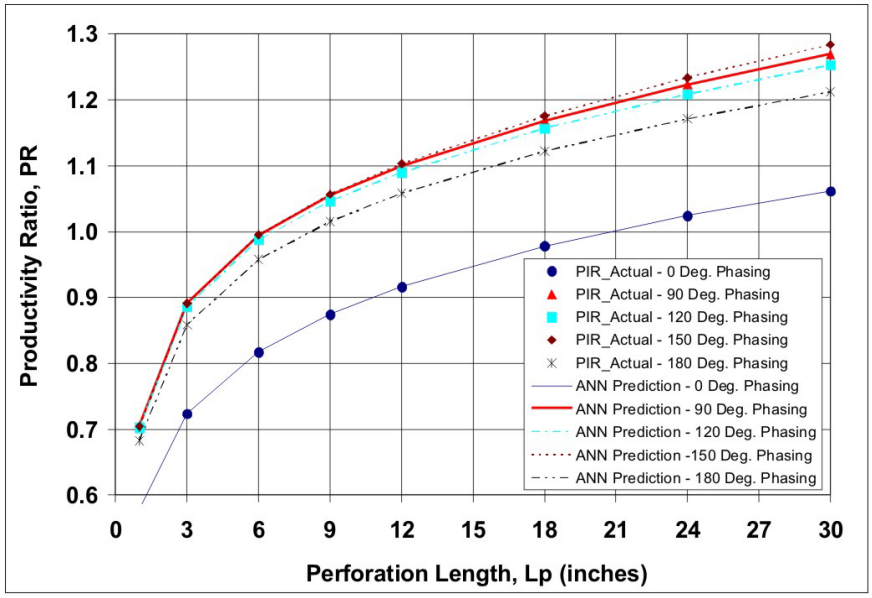

Figure 14. Comparison of ANN predictions and WIM base case results for 0°, 90°, 120°, 150°, and 180° phasing angles

Figure 15 shows FEA results along with the neural network results when r_w and D_{EH} are fixed at 4.25 in. and 0.5 in., respectively. In this plot, shot phasing is held constant at 60 degrees. Each curve represents productivity ratio as a function of perforation length when different shot densities are used. The neural network results show excellent correlation with the results obtained from WIM.

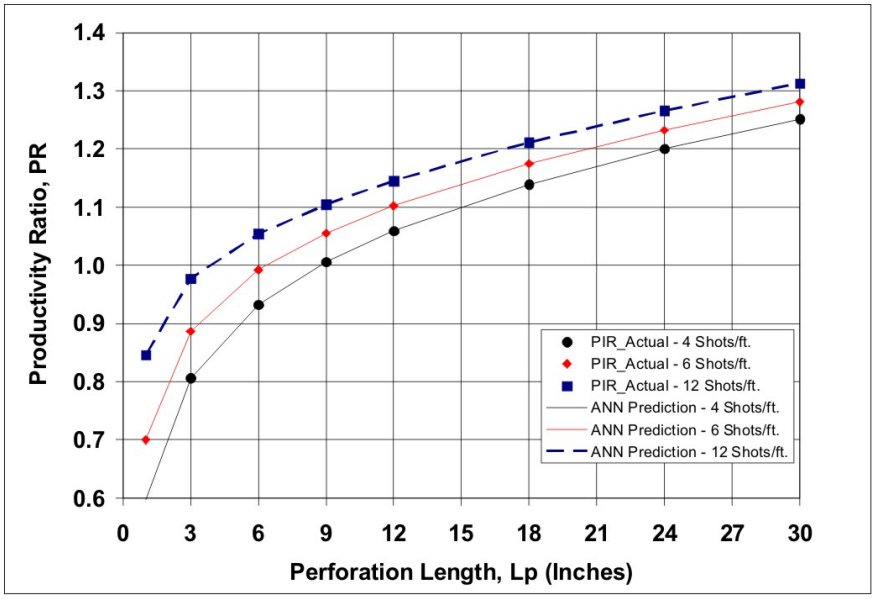

Figure 15. Comparison of ANN predictions and WIM results for different shot densities

Computation speed is extremely fast for the network and can easily be programmed into a spreadsheet or stand-alone computer application for optimizing perforated completions. This eliminates the need for a time-consuming and costly FEA run each time that a new perforating pattern needs to be evaluated. The ANN algorithm is incorporated into a new perforation design optimization software, PerfPro™, which is described next.

PerfPro Software – Application

PerfPro™ was developed as an engineering tool for optimizing perforation design and for evaluation of the efficiency of cased and perforated wells. The software offers a unique combination of features that allows for quick assessment of the effect of perforation parameters on the overall inflow performance of a well. It incorporates productivity results of the FE runs with an efficient ANN algorithm.

PerfPro has a user-friendly graphical interface that allows users to enter data, launch the calculations, and analyze the results. Figure 16 shows a snapshot of one of the screens of PerfPro preprocessor. The core simulation module is extremely fast and calculation of productivity and pseudo-skin for a given completion scenario only takes seconds. In addition, the graphics produced by the PerfPro postprocessor allows design results to be clearly presented and quickly interpreted.

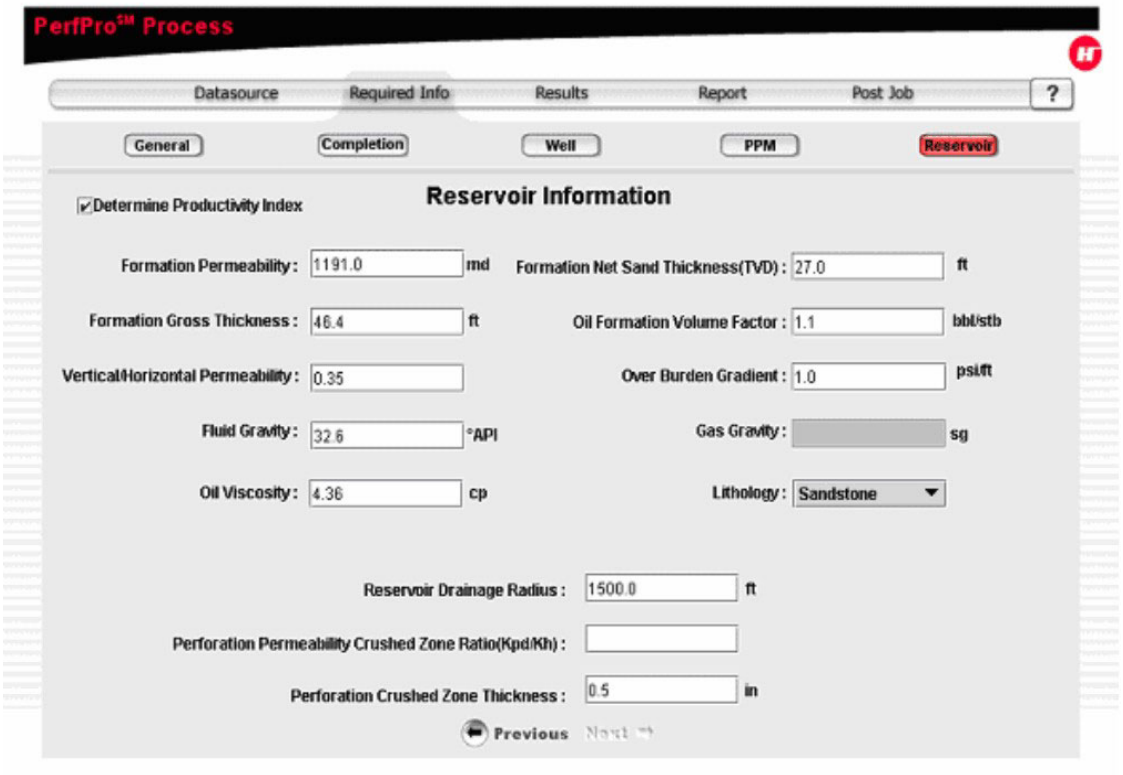

Figure 16. PerfPro preprocessor (input) screen

The example provided below involves an offshore GOM oil well that was perforated with 350 psi underbalance and a DST was performed to determine reservoir properties. Efficiency of the perforating design was examined with evaluation of charge performance and well productivity, given the following wellbore and reservoir parameters:

Casing Size:	9-5/8” (Perforated Underbalance with TCP Guns)
Perforations:	2701 to 3603 ft. (Measured Depth)
Gun Type:	4-1/2” 12 SPF DP Scalloped Guns
Bottomhole Pressure:	1500 psi

Bottomhole Temperature:	112 ° F
Average Permeability:	1200 md
Reservoir Porosity:	24 %
Well Deviation:	52 deg
Oil Gravity:	32 API
Average Gas-Oil-Ratio:	500 Scf/Bbl

Performance of the 4-1/2-inch 12 SPF gun used to perforate the well is presented in Table 1, and plotted in Figure 17. A sensitivity analysis was performed to evaluate if any increases in well productivity were achievable with upgrading the gun system to a 7" OD 12 SPF deep penetrating gun system. Thus, two additional gun systems were considered, in addition to the 4-1/2-inch deep penetrating scalloped gun (**Table 2**). Results of the PerfPro analyses are presented in **Table 3**. One of the screens of the PerfPro postprocessor is shown in Figure 18.

Table 1. 4 ½-inch Gun (Gun 1) Perforation Shot Performance

Gun/Charge Type	4-1/2" DP		**Avg Formation Penetration**		25.74 in			
Gun Position	Eccentered		**Avg Exit Hole Diameter**		0.34 in			
Shot Phasing	45 deg							
Shot No.	1	2	3	4	5	6	7	8
Orientation, deg	0.0	45.0	90.0	135.0	180.0	225.0	270.0	315.0
Gun Clearance, in	0.0	0.35	1.55	3.31	4.18	3.31	1.55	0.35
Formation Penetration, in	26.71	26.6	26.0	24.86	24.26	24.86	26.0	26.6
Exit Hole Dia 1st Csg, in	0.35	0.35	0.35	0.35	0.35	0.35	0.35	0.35

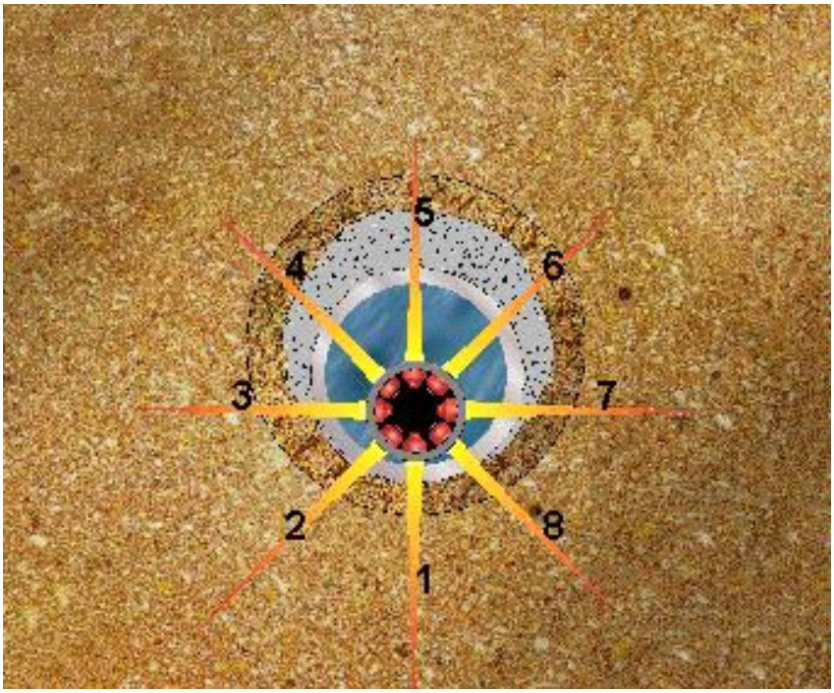

Figure 17. Gun 1 (4 ½" DP) charge performance plot

Table 2. Perforator Information on Guns used in Sensitivity Analysis

Gun #	Gun 1	Gun 2	Gun 3
Charge Name	4-1/2" DP	7" MILLENNIUM	7" MILLENNIUM
Gun Position	Eccentered	Eccentered	Eccentered
Shot Phasing, deg	45.0	45.0	45.0
Shot Density, spf	12	12	12
Avg Formation Penetration, in	25.74	40.84	40.84
Avg Exit Hole Diameter, in	0.34	0.36	0.36
Underbalance Condition, psi	-350.0	-350.0	-750.0

Table 3. Productivity Results from the Sensitivity Analysis

Gun #	Total Skin	Perforation Skin	Productivity Index, Stb/Day/psi
Gun No 1	0.024	0.721	6.515
Gun No 2	-0.672	0.025	7.206
Gun No 3	-0.774	-0.077	7.319

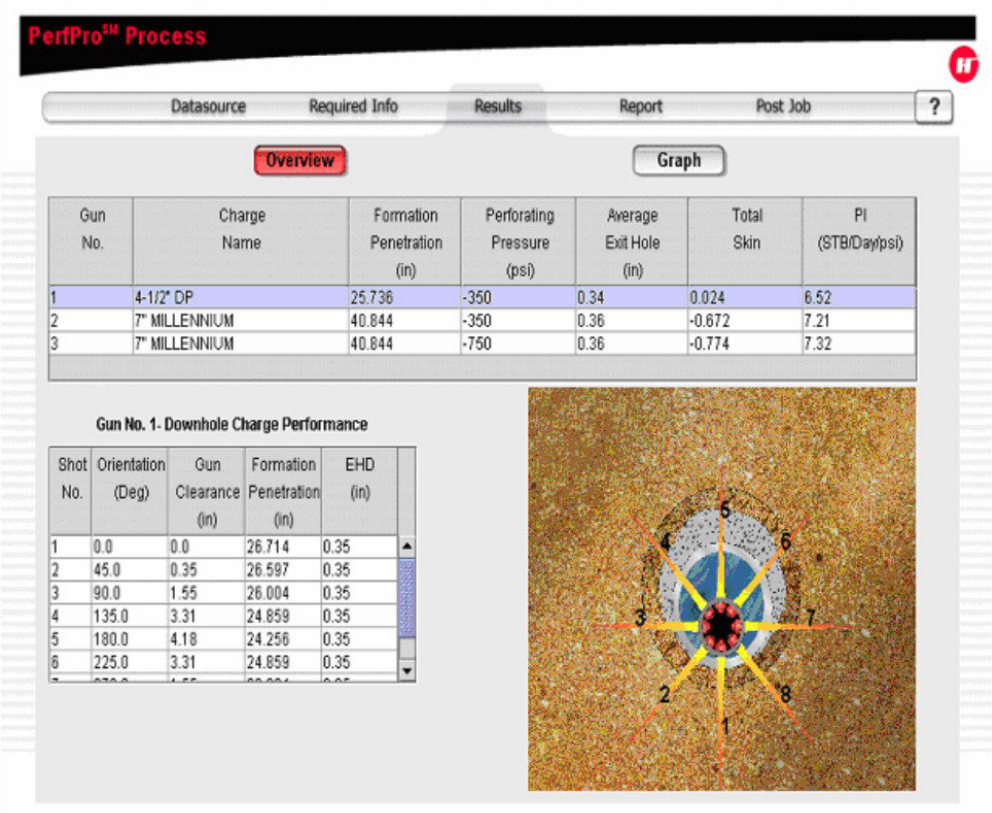

Figure 18. PerfPro output (postprocessor) screen

As can be seen from the "productivity analysis", small increases in well productivity are possible, although the increases are minimal. A pressure transient analysis was performed with the DST pressure gauge information to evaluate formation permeability and skin effect due to perforating. Review of the DST results reveals a completion with permeability of 1191 md and total skin factor of zero. Note that these results compare favorably with the PerfPro perforating design results and validate the charge performance simulation.

The key component in being able to match the actual field results is the method by which the theoretical perforating models handle the way in which the perforation event is performed. A proprietary perforating algorithm takes into account the degree of over or under-balance pressure during perforating to calculate an effective perforation tunnel length. A drilling damage radius of 8" and anisotropy of 0.35 were assumed for this analysis. As part of optimizing the perforating process post-job perforating information is collected and analyzed to continuously validate the perforating models in the software. The post-job information provides the basis for a perforating database, in which reservoir or completion specific perforating recommendations can be provided based on empirical data to support the theoretical perforation modeling.

Conclusion

A new perforation performance prediction model has been introduced for optimizing the design of cased and perforated well completions. The model is very efficient and the results have been tested successfully against previously published data. Based on results from preliminary application of the new model, the following conclusions can be drawn:

- The artificial neural network model introduced in this work provides efficient means of optimizing a completion design by quickly analyzing a large number of FEA simulated completion scenarios.
- Several primary and secondary factors, including perforation length, casing entrance hole diameter, crushed zone properties, formation anisotropy, dip angle of the bedding planes, etc., affect the productivity of a perforated well.
- The complex interaction of these primary and secondary factors calls for optimization in the design of perforated completions that will result in maximizing inflow performance of a well. This optimization should take into account the unique properties of the reservoir.
- Application of the new software is demonstrated by the field example given in this paper.

Nomenclature

c_t = total reservoir compressibility
D_{EH} = casing entrance hole diameter
d_p = perforation diameter at the reservoir sand face
d_t = hole diameter at the tip of perforation
h = formation thickness
J = well productivity index
k = average permeability
k_{xx} = mobility in the x-direction
k_{xy} = average horizontal permeability (in x-y plane)
k_{yy} = mobility in the y-direction
k_z = vertical permeability
k_{zz} = mobility in the z-direction
p = reservoir pressure
q = production rate
r_e = radius of the external boundary
r_w = wellbore radius
s_t = total skin factor
s_D = drilling-induced skin damage

s_{pc} = skin due to partial completion
s_{pf} = perforation skin factor
s_{θ} = skin due to well deviation

Greek Symbols

ϕ = average porosity
μ = viscosity of reservoir fluid
θ = phase angle
θ_{dip} = dip angle of the reservoir anisotropy

Acknowledgements

The authors wish to thank the management of Halliburton Energy Services for permission to publish this paper.

References

1. McDowell, J.M. and Muskat, M.: "The Effect on Well Productivity of Formation Penetration Beyond Perforated Casing ," *Trans.* AIME 189 (1950) 309-12.
2. Harris, M.H.: "The Effect of Perforating on Well Productivity," *JPT* (April 1966) 518-28.
3. Klotz, J.A., Krueger, R.F., and Pye, D.S.: "Effect of Perforation damage on Well Productivity," *JPT* (Nov. 1974) 1303-14.
4. Cinco, H., Miller, F.G., and Ramey, H.J.: "Unsteady Pressure Distribution Created by a Directionally Drilled Well," *JPT* (Nov. 1975) 1392-1400.
5. Saidikowski, R.M: "Numerical Simulations of the Combined Effects of Wellbore Damage and Partial Penetration," paper SPE 8204 presented at the 1979 Annual Technical Conference and Exhibition, Las Vegas, Sept. 23-26.
6. Karakas, M. and Tariq, S.M.: "Semianalytical Productivity Models for Perforated Completions," *SPEPE* (Feb. 1991) 73-82.
7. Hong, K.C.: "Productivity of Perforated Completions in Formations With and Without Damage," *JPT* (Aug. 1975) 1027-38.
8. Locke, S.: "An Advanced Method for Predicting the Productivity Ratio of a Perforated Well," *JPT* (Dec. 1981) 2481-88.
9. Tariq, S.M.: "Evaluation of Flow Characteristics of Perforations Including Nonlinear Effects with the Finite Element Method," *SPEPE* (May 1987) 104-12.
10. Dogulu, Y.S.: "Modeling of Well Productivity in Perforated Completions," paper SPE 51048 presented at the 1998 SPE Eastern Regional Meeting, Pittsburg, PA, Nov. 09-11.
11. API RP 43, Recommended Practices for Evaluation of Well Perforators, fourth edition, American Petroleum Institute, Washington, DC (1985).
12. Ansah, J., Proett, M.A., and Soliman, M.Y.: "Advances in Well Completion Design: A New 3D Finite-Element Wellbore Inflow Model for Optimizing Performance of Perforated Completions," paper SPE 73760 presented at the 2002 SPE Symposium on Formation Damage Control in Lafayette, LA, Feb. 20-21.